J Nanostruct Chem (2015) 5:333–346
DOI 10.1007/s40097-015-0165-y

ORIGINAL RESEARCH

Photodegradation of dye acridine yellow on the surface of mesoporous TiO_2, SiO_2/TiO_2 and SiO_2 films: spectroscopic and theoretical studies

N. P. Smirnova[1] · N. I. Surovtseva[1] · T. V. Fesenko[1] · E. M. Demianenko[1] · A. G. Grebenyuk[1] · A. M. Eremenko[1]

Received: 26 March 2015 / Accepted: 20 June 2015 / Published online: 28 July 2015

Abstract Electronic spectra and LDI mass spectra changes accompanying photodegradation of acridine yellow (AY) adsorbed on the surface of prepared via templated sol–gel synthesis TiO_2, SiO_2, and TiO_2/SiO_2 mesoporous films have been investigated and the main photodegradation products have been determined. The results of calculations show the adsorption energy of the molecular state of AY to be the greatest for the complex with titania–silica where Lewis acidic sites are present, the smallest one being related to the complex with titania what corresponds to the experimental data. Effectiveness of acridine yellow photodegradation on the surfaces of mesoporous films under UV irradiation increases in a row $SiO_2 < TiO_2/SiO_2 < TiO_2$. Electronic and laser desorption/ionization mass spectra and theoretical modeling give evidence that efficient photobleach of AY localized at the surface of anatase films proceeds through the following steps: 1—*N*-demethylation/deamination; 2—photodimerization; 3—photodegradation.

Keywords Acridine yellow · Adsorption · Aggregation · Photodegradation · Mesoporous TiO_2 · SiO_2 and TiO_2/SiO_2 films · Quantum chemistry simulation · UV–Vis · Laser desorption–ionization mass spectroscopy

✉ N. P. Smirnova
smirnat@i.ua

[1] Chuiko Institute of Surface Chemistry of National Academy of Sciences of Ukraine, General Naumov Str., 17, Kiev 03164, Ukraine

Introduction

Acridine dyes have ubiquitous use as colorant for synthetic fibers, tissue, leather, fluorophores with high fluorescence intensity in luminescent analysis [1–3]. The creation of novel antitumoral medications for chemio- and photodynamic therapy is focused on acridine dye [3]. A significant photodynamic effect and antimicrobial activity are observed in the presence of light and oxygen. Acridine derivatives such as acridine yellow (AY) are promising as photosensitizers for energetical projects: photocatalytic hydrogen evolution [4], solar photocatalysis [5], and solar cell production [6].

Gradual improvements of solar cell and photocatalyst efficiency have been achieved with the development of the synthetic route to prepare the mesoporous TiO_2 film consisting of nanosized semiconductor particles or TiO_2/SiO_2 nanocomposite films where silica matrix provides the transport of reagents to TiO_2 nanoparticles via developed porous structure. Mixed oxide composite materials can often be more efficient photocatalysts than pure substances through the generation of new active sites and improved mechanical strength, thermal stability and surface area of titania [7, 8]. After band gap excitation of titania, photogenerated electrons and holes migrate to the particle surface, from where they can participate in electron transfer reactions with adsorbed molecules. Titanium ions in mixed silica–titania compositions are also available for the local electron–acceptor interaction with the adsorbed excited organic molecules. It can create a competing deactivation pathway for the excited organic molecules.

The active surface area and adsorption capacity to the molecular sensitizer (dye) are greatly increased in such systems resulting in an effective light absorption [8–10]. A common problem associated with the majority of organic

dyes is their tendency to form aggregates on the surface of the semiconductors that significantly change the absorption spectrum and other photophysical properties of mentioned system [11, 12] and complicate the interpretation of results.

Besides that, acridine dyes are wide-spread pollutants of the drugs, textile and photographic industry. Detailed knowledge on photostability and photodecomposition of dyes adsorbed on the oxide surfaces in air is desirable to monitor the intermediates of the destruction [13, 14].

Thus, we focused on the mechanism and products of photodegradation of adsorbed dye—acridine yellow (AY) on three reactive surfaces such as mesoporous TiO_2, SiO_2, and TiO_2/SiO_2 films.

Generally accepted experimental methods are not always able to elucidate elementary stages of the reactions as well as the structures of adsorption complexes. Our previous studies [15–17] have demonstrated the feasibility of using optical transparent mesoporous sol–gel films with developed surface area as a substrate for matrix-free LDI-MS analysis that gives us a possibility for in situ investigation of phototransformations of adsorbed dye. To verify the probable routes of photodegradation of organic dyes, in our case acridine yellow, theoretical simulation such as quantum chemistry can be used.

Experimental

The transparent porous thin films with the developed porosity and the high surface area were synthesized via low-temperature sol–gel route in presence of template agents as was described in the previous studies [16, 18, 19]. We prepared acid catalyzed silica and titania sols from tetrapropylorthotitanate [Ti $(OC_3H_7)_4$, used as TiO_2 source], tetraethoxysilane [$Si(OC_2H_5)_4$, used as SiO_2 source]. Hydrochloric acid in water was used as the catalysts, and de-ionized water for hydrolysis, using commercially available triblock copolymer polyethylene oxide–polypropylene oxide Pluronix P123 (BASF) as template. To control hydrolysis–condensation reaction rates and to prevent oxides precipitation, acetylacetone was used as a complexing agent. Silica–titania (10 wt% TiO_2) was prepared via addition of TiO_2 (anatase, 7 nm) nanoparticles stabilized by 2-methoxyethoxide [20] to SiO_2 sol after prehydrolysis. TiO_2 nanoparticles were prepared from stable TiO_2 hydrosols obtained via hydrolysis of titanium tetra(2-methoxyethoxide), dried under room temperature and heat treated at 80 °C similar to that in [20]. Dip-coating procedure was used for film formation on glass substrate. Thermal treatment of films was made at 350. TiO_2 films were than treated at 500 °C to ensure the anatase phase formation.

The Brunauer–Emmett–Teller (*BET*) *surface area* and pore size distribution of the thin film were measured from hexane adsorption–desorption isotherms. The film weight was calculated by subtracting the weight of the substrate (covering slides for microscopy) from that of TiO_2-coated sample.

Hydrophilic properties of films were estimated by measurements of water contact angle using the sessile drop method with a MIR-1 microscope (LOMO, St. Peterburg, Russia). Thus, a drop of distilled water was applied to a film covered on glass slide previously heated for 0.5 h at the temperature of 350 or 500 °C. Measurements were carried out in air at room temperature (20 ± 2 °C).

Photobleach procedure films with adsorbed dye were exposed to the influence of a mercury lamp light. Before an irradiation, films were dried an air at 50–100 °C to remove solvent. Studies of a photobleach of adsorbed dyes were carried out at the acridine yellow (AY) amount within the limits of $1–1.5 \times 10^{-4}$ M/g of film with equal optical density in the AY absorption. Irradiation density with mercury lamp was 10^{17} quant/cm^2 of films. For each sample, the initial absorption spectra were obtained. Then, they were taken as a function of the exposure time.

LDI measurements under laser desorption/ionization mass spectrometry (LDI) experiments the positive (negative in the case of SiO_2/TiO_2)-ion mass spectra were acquired using an Autoflex II (Bruker Daltonics Inc., Germany) mass spectrometer. The samples were irradiated with a 337-nm nitrogen laser operated at 20 Hz (3 ns pulse duration) and attenuated with neutral density filter. A delayed extraction period of 10 ns was used to minimize the energy spread of the ions for optimum resolution then the ions were accelerated by 20 kV pulse through a reflectron time-of-light analyser and detected using a multichannel plate detector [15, 16].

Results and discussion

Morphological properties and phase structure of prepared films

Hexane adsorption–desorption isotherms and pore size distribution analysis of the mesoporous TiO_2, TiO_2/SiO_2 and SiO_2 films are illustrated in Fig. 1.

Isotherms of hexane adsorption on the films are of type IV which indicates the presence of mesopores [21]. For TiO_2/SiO_2, SiO_2 films calcined at 350 °C, and TiO_2 at 500 °C adsorption–desorption isotherms have two hysteresis loops: the first one at high pressures of hexane which indicates the presence of mesopore and the second loop at low pressures, which indicates the irreversible structural deformation of films and formation of the so-

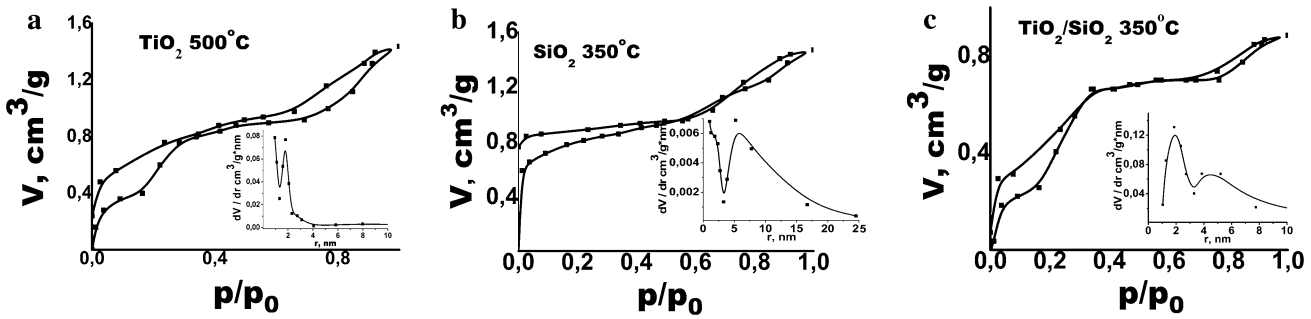

Fig. 1 Hexane adsorption isotherms, and the distribution function of pore size—*insets* of SiO_2 (**a**), SiO_2/TiO_2—10 % (**b**) film on glass substrate sintered at 350 °C and TiO_2 film (**c**) sintered at 500 °C

Table 1 Hydrophilic properties and efficiency in AY photodegradation of SiO_2, SiO_2/TiO_2 and TiO_2 films

Sample	S_{BET} m^2/g	D, nm	Water contact angle, grad		Adsorption AY, mol/g of the film	Rate constants of adsorbed AY decomposition $k \times 10^{-2}$, min^{-1}
			Before	After 10 min UV		
SiO_2 350 °C	1580	<2; 12	10	10	2.2×10^{-4}	0.6
TiO_2/SiO_2 350 °C	1300	4; 10	12	5	2.9×10^{-4}	3.5
TiO_2 500 °C	910	<2; 4	10	~0	1.8×10^{-4}	15

called ink bottle type of porosity [22]. In this case, desorption of adsorbed molecules is hindered at a given temperature. Moreover, the shape of the hysteresis loop for SiO_2 nanocomposite clearly indicates the presence of micropores in this sample. The total surface area and effective pore radii values yielded from BET analysis of the isotherms are presented in Table 1.

The shape of the adsorption–desorption isotherms and pore size distribution of prepared TiO_2, TiO_2/SiO_2 and SiO_2 films indicate the presence of pores of different diameters. Thus, the pore diameters of 4 and 10 nm dominate in TiO_2/SiO_2 films. Both TiO_2 and SiO_2 samples have micropores with diameter of less than 2 nm and mesopores with diameter about 4 and 12 nm, respectively. The effective pore radius of the TiO_2 films, calculated from the corresponding SEM images (not shown), was ~8–12 nm.

Anatase phase has been identified in XRD patterns for TiO_2 and TiO_2/SiO_2 ($d \sim 7$ nm) powders prepared from films precursors (Fig. 2).

Hydrophilic properties of the synthesized films

SiO_2 and TiO_2/SiO_2 films freshly prepared on glass substrates showed highly hydrophilic properties (see data listed in Table 1); water contact angles for them were ca. 10°–20°. TiO_2 films after calcination at 350 °C show contact angle near 32°. Thermal treatment at 500 °C leads to a drop of water contact angle up to 5°–10°. Literature data on the contact angle of water on a clean titania surface are contradictory, ranging from 72° reported in [23] to 33.3° in [24] and 15° in [25] depending on the film structure and storage conditions. Various experimental results relating to this phenomenon have shown that it is caused by defects formed on the surfaces of the as-prepared TiO_2 thin films subjected to high-temperature calcination, especially in case of template syntheses involving high level of organic component as it was used in our work. According to K. Hashimoto and co-workers, the wettability of TiO_2 surfaces can be altered by irradiation [23–25]. After UV illumination (10 min in air under mercury lamp light), mesoporous TiO_2 films exhibited photoinduced super-hydrophilic properties with water contact angle near 0°.

FTIR investigation

The FTIR spectrum of TiO_2 (500 °C) powder prepared from the film precursor contains a single broad high-intensive absorption band at 1000–370 cm^{-1} with a maximum at 550 cm^{-1} associated with the Ti–O stretching vibrations. In the FTIR spectra of the mesoporous SiO_2 and TiO_2/SiO_2 calcined at 350 °C (Fig. 3) a set of vibrations can be seen as characteristic of the materials studied. The band at 794–804 cm^{-1} is assigned to symmetric stretching vibrations of the Si–O–Si bond [26–29]. Intensive band at 947–960 cm^{-1} is usually attributed to the stretching vibrations of the Si–O–Ti bond [27–29] for TiO_2/SiO_2 mixed oxides prepared through simultaneous hydrolysis of the titanium and silicon containing organometallic

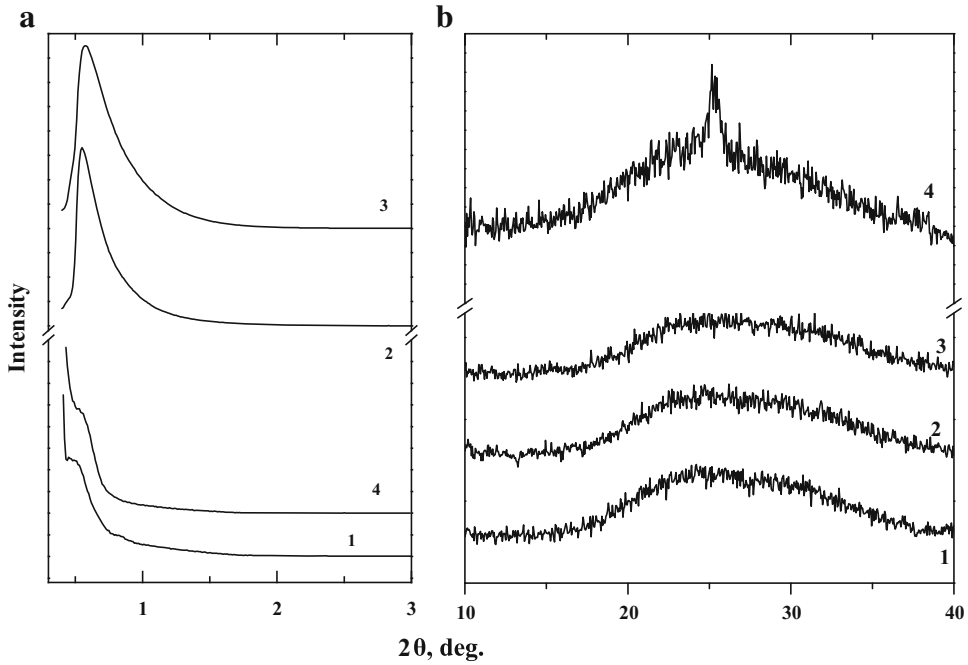

Fig. 2 Low-angle X-ray diffraction patterns (**a**) and wide-angle XRD patterns (**b**) of the meso-structured SiO_2—1, SiO_2/TiO_2 (10 %)—2 and TiO_2 films calcined at 350 °C—3, at 500 °C—4

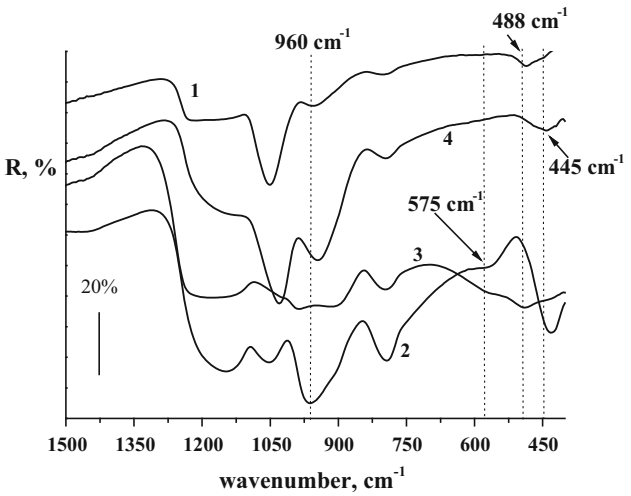

Fig. 3 FT-IR spectra of the mesoporous SiO_2 (1) and TiO_2/SiO_2 (2–1 mol.% of TiO_2; 3–5 mol.% of TiO_2; 4–10 mol.% of TiO_2) films deposited onto steel substrates and calcined at 350 °C

precursors. This shows evidences of chemical interaction between titania and silica at molecular level. When titania nanoparticles containing 2-methoxyethoxide side groups interact with growing Si–O–Si chain, Si–O–Ti bonds can be formed at the interface.

A weak band in the range of 952–958 cm^{-1} is also seen in the FTIR spectrum of pure SiO_2 and is assigned to the symmetric stretching vibrations of the Si–OH groups [27, 28]. Two bands in the range of ~1023–1041 cm^{-1} and ~1146–1192 cm^{-1} are attributed to the asymmetric stretching vibrations of the Si–O–Si bond [27–29]. It is accepted that degree of titanium incorporation into silica framework can be monitored by the intensity of the band at ~960 cm^{-1} corresponding to the vibrations of the Si–O–Ti bond [29]. In our case, intensity of the band gradually decreases with increasing titanium content into silica framework from 1 to 10 mol.% that can be related to the titania polymer network formation and/or titania segregation into separate phase in the SiO_2 network with increasing its content in the mixed oxides. The presence of two bands in the wave numbers range 440–480 and 550 cm^{-1} in the IR spectrum of the titanosilicates evidences of the formation of zeolite-type structure in this system [30, 31]. First band corresponds to the internal vibrations of the Si–O tetrahedrons and is also presented in the spectrum of pure SiO_2. It corresponds to the stretching vibrations of the Si–O–Si bond. In the FTIR spectrum of the mesoporous SiO_2 film (Fig. 3, curve 1), one band can be seen in the range of 484–488 cm^{-1}. When titania was added (1, 5 mol.%) into SiO_2 films (Fig. 3, curves 2, 3), we registered two bands of low intensity: the first one at 563–575 cm^{-1} and the second one at ~432–490 cm^{-1}. First band is similar to that of five-membered rings of Si–O–T (where T = Si or Ti) in microporous zeolites [30, 31]. On the assumption of the integral intensity of the bands of adsorbed water at 1640 cm^{-1} and associated water molecules with surface hydroxyl groups in the range of 3600–3300 cm^{-1} we can make a conclusion about surface hydroxylation of the films depending on the TiO_2 content in the SiO_2 matrix. It was observed the increase of the surface hydroxylation of

titanium-containing silica in comparison with bare SiO_2 films after similar thermoactivation. According to [26], the reduction in the absorption frequency of Si–O stretching vibration (near 1100 cm^{-1}) indicates the distortion of a SiO_4 tetrahedron in the presence of a heavier neighboring atom linked to a tetrahedron via an oxygen atom. The formation of Ti–O–Si bonds is assumed to be a key factor affecting surface properties such as step of surface hydroxylation and surface acidity and catalytic function of silica–titania [9, 10, 32]. Imamura et al. [10] reported the change in the amount of acid sites of silica–titania with the change in Ti:Si ratio: weak acid sites were present on both single component oxides. Stronger acid sites appeared after their combination. Maximum amount of sites with acid strength of $1.5 < H_o \leq 3.3$ was observed for TiO_2/SiO_2 with low Ti content up to 10 %.

As we reported previously analysis of the data of XPS investigation of the mixed TiO_2/SiO_2 as well as bare titania and silica films [33] proved molecular scale mixing for sol–gel derived titanosilicates. Considerable upward shift of the $Ti2p_{1/2}$ and $Ti2p_{3/2}$ lines was registered for TiO_2/SiO_2 film as compared with lines position for pure TiO_2. This upward shift can account for the formation of the Ti–O–Si bonds, as a result of increase of the positive charge on the Ti species resulting from the greater electronegativity of Si via O acting on Ti [28]. Downward shift of the position of O*1s* and Si*2p* lines for TiO_2/SiO_2 film was detected relatively to the position of the lines for pure SiO_2 film. Lee et al. [27] explained this negative O*1s* line shift to the insertion of the Ti^{4+} cations into the tetrahedral sites of the silica network to form Ti–O–Si bonds.

Theoretical studies on acridine yellow adsorption and photodegradation on silica, silica–titania, and titania surfaces

When organic substances are adsorbed on silica and titania surfaces, the reactivities of their molecules can change as compared to those in free state.

Elementary stages of reactions as well as the structures of adsorption complexes not always can be determined by experimental methods. To verify probable photodegradation routes of organic dyes, in particular those of acridine yellow, theoretical simulation can be used, especially methods of quantum chemistry [34]. Density functional theory method (DFT) is used successfully in studies of the mechanisms of both homolytic and heterolytic decomposition of organic matter [35], as this method describes electron correlation.

Our previous calculations testify [36] the use of B3LYP functional with extended valence-split 6–31G(d,p) basis set in calculations of energy values of reaction mechanisms to give reasonable results and negligible the basis set superposition error as compared to other, more improved methods. That is why the calculations were performed using the DFT method with B3LYP exchange–correlation functional and 6-31G(d,p) basis set [37, 38]. The dispersion correction was taken into account using the DFTD3 model by Grimme et al. [39]. The equilibrium spatial structures of reactant molecules and reaction products of the elementary stages were found due to gradient norm minimization. All the calculations have been carried out by means of the US GAMESS program [40].

First, probable adsorption complexes are to be examined of AY (in neutral and protonated HAY^+ forms) on the surfaces of the sorbents.

The energy values of acridine yellow adsorption on silica, titania–silica, and titania surfaces were found according to Hess law from the total energy values for calculated models as follows:

$$\Delta E_{\text{ads}} = E_{\text{total ads. comp.}} - (E_{\text{total surface}} + E_{\text{total AY}}).$$

To elucidate the size effect of the surface model on the energy of adsorption, three adsorption complexes were examined of AY molecule on silica surface. The silica surface was simulated with a unit of polysilicic acid containing 5, 6, and 7 silicon–oxygen tetrahedra terminated by hydroxyl groups (Fig. 4). According to the results of calculations, when models for silica surface are polysilicic acids containing 6 and 7 silicon–oxygen tetrahedra (their linear dimensions are greater than that of adsorbate molecule), there is no considerable difference in the values of adsorption energy. Therefore, we use models for oxide surfaces fit in size to the AY molecule.

The silica surface was simulated with a unit of polysilicic acid of $Si_5H_{12}O_{16}$ containing 5 silicon–oxygen tetrahedra terminated by hydroxyl groups (Fig. 5) [41].

The titania–silica surface in the adsorption complex formed by Brønsted sites was simulated by a $TiSi_4H_{12}O_{16}$ structure containing one titanium–oxygen and four silicon–oxygen tetrahedra terminated by hydroxyl groups (Fig. 6).

The model of titania–silica with strong Lewis acidic sites is formed due to water molecule addition to the previous model (Fig. 7). In the model obtained, the hydrogen atom of water molecule is connected to the bridge oxygen atom (between titanium and silicon atoms) and the OH group joins titanium atom to enlarging its coordination number to five.

The model of titania–silica with weak Lewis acidic sites is formed from the previous model due to removal of the water molecule: $TiSi_4H_{12}O_{16} - H_2O \rightarrow TiSi_4H_{10}O_{15}$ (Fig. 8) [42] whereas titania surface was simulated by a fragment of anatase face(100) stabilized by four water molecules (Fig. 9) [43, 44].

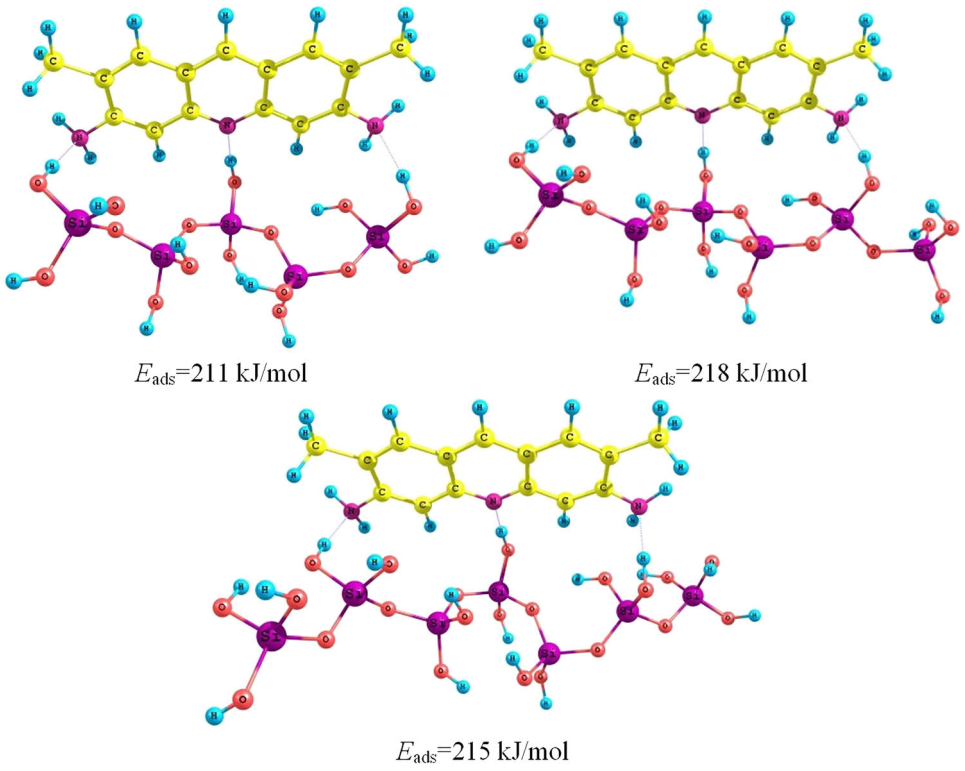

Fig. 4 Adsorption complexes of acridine yellow in molecular form with silica surface which containing 5, 6, and 7 silicon–oxygen tetrahedra

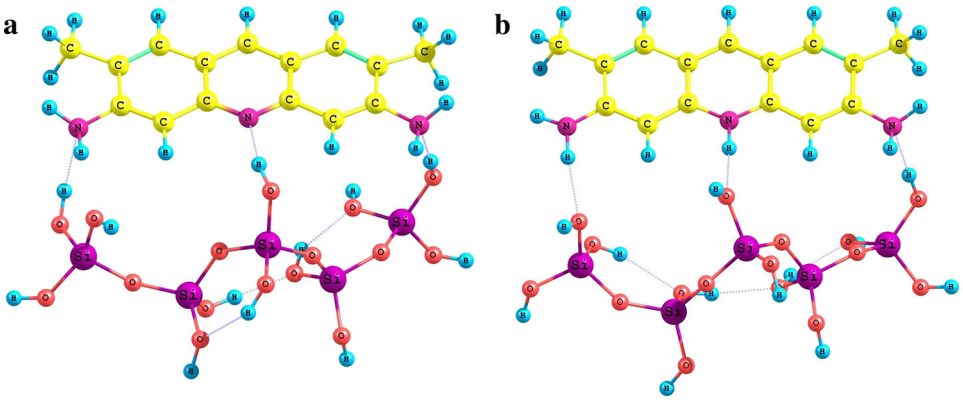

Fig. 5 Adsorption complexes of acridine yellow in molecular (**a**) and protonated (**b**) forms with silica surface

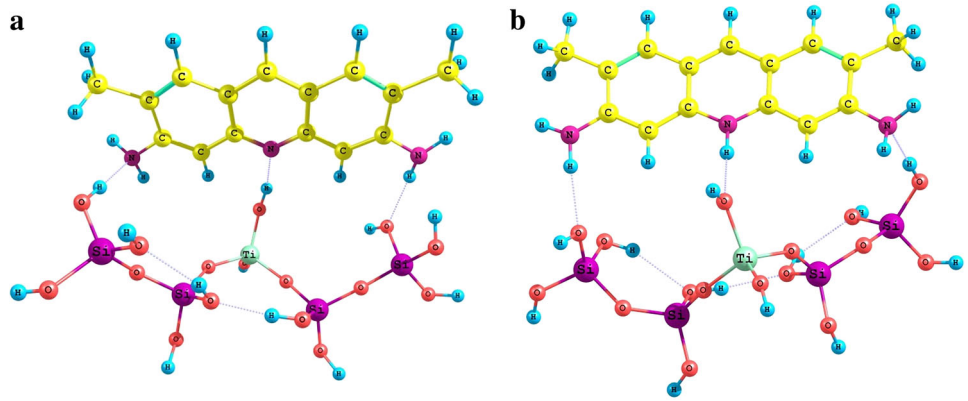

Fig. 6 Adsorption complexes of acridine yellow in molecular (**a**) and protonated (**b**) forms with titania–silica surface with a weak Brønsted site

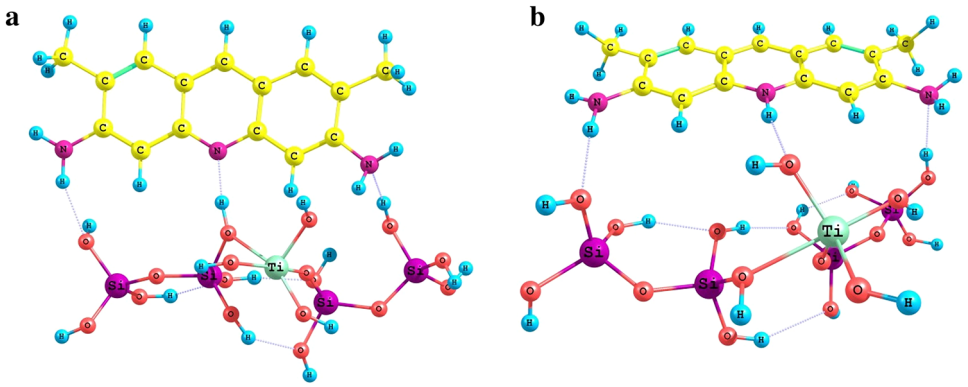

Fig. 7 Adsorption complexes of acridine yellow in molecular (**a**) and protonated (**b**) forms with titania–silica surface with a strong Brønsted site

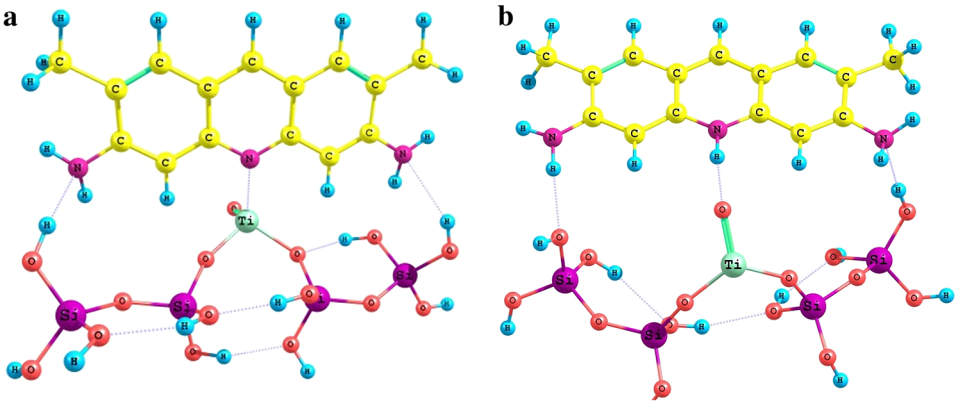

Fig. 8 Adsorption complexes of acridine yellow in molecular (**a**) and protonated (**b**) forms with titania–silica surface with a Lewis acid site

When acridine yellow molecule is adsorbed, its pyridine-type nitrogen atom forms bonds with both Brønsted and Lewis surface acidic sites of the substances mentioned above.

The results of calculations (Table 2) show the adsorption energy of the molecular state of AY to be the greatest for the complex with titania–silica where Lewis acidic sites are present, the smallest one being related to the complex with titania what corresponds to the experimental data [45]. For AY–H^+, the greatest adsorption energy relates to its interaction with titania surface, whereas the smallest one is a characteristic of titania–silica surface with Lewis acid sites.

Along with examination of the structures of adsorption complexes, the basicities have been analyzed of both amine-type and pyridine-type nitrogen atoms in acridine yellow molecule via comparing their proton affinity values [46]. The results of calculations prove the proton affinity of pyridine-type nitrogen atom (1146 kJ/mol) to be for 183 kJ/mol greater than that of amine-type one (963 kJ/mol).

Besides, two probable routes have been examined of acridine yellow photodegradation with similar reaction products.

The energy effects of related routes of photochemical destruction were evaluated analogously to the adsorption energy values; the total energy values of reactants and reaction products were calculated for their triplet states as we assumed the lifetimes of the structures mentioned in the excited singlet states to be too small for the reaction to take place as compared with that of the first triplet state [47].

The total energy values for reaction products were calculated for various multiplicities; the minimum total energy value was found to relate to the quadruplet for the first route whereas it related to triplet for the second one.

Table 3 shows the energy effects of the probable routes of gas phase acridine yellow destruction; it is seen from the results of calculations that photodegradation of free acridine yellow occurs according to the first route as independent on the calculation method used.

Table 4 shows the energy effects for acridine yellow photodegradation on silica, titania–silica, and titania surfaces calculated with use of method B3LYP-D3/6–31G(d,p).

For adsorbed acridine yellow, each route of photodegradation can occur in two ways (Fig. 10).

In the first case (Fig. 10a), one reaction product (1) is adsorbed on the surface and another one (2) is in a free state. In the second case (Fig. 10b), vice versa, the reaction product (2) is adsorbed on the surface whereas the product (1) is in a free state.

Under conditions of mass spectrometry experiment, elimination of methyl group (Fig. 11a) or aminogroup (Fig. 11b) from acridine yellow molecule can occur.

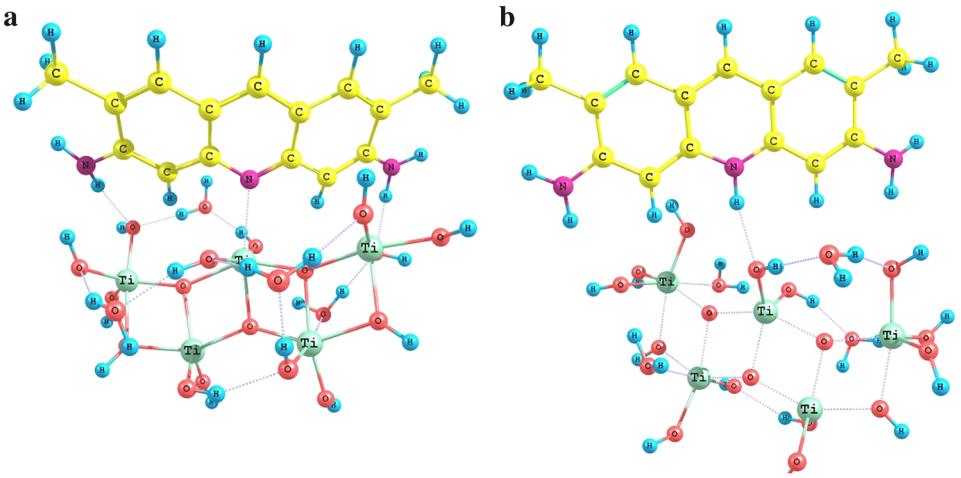

Fig. 9 Adsorption complexes of acridine yellow in molecular (**a**) and protonated (**b**) forms with titania surface [a fragment of anatase face(100)]

According to the results of quantum chemical calculations, the energy effect values of these two routes (Fig. 11) are almost the same as follows: methyl group separation needs 383.2 kJ/mol and that of amino group needs 387.1 kJ/mol. This fact testifies to uniform probability of acridine yellow destruction according to these two routes.

It has been found on the base of the results of quantum chemical calculations that acridine yellow is best adsorbed on titania–silica surface where Lewis sites play a key role whereas it is less adsorbed on titania (anatase) surface. The gas phase destruction of acridine yellow has been found to occur due to formation of the fragments with odd number of electrons. The destruction route preferred is independent on the surface nature. The photodegradation of acridine yellow has been found to occur most easily on the titania surface. In agreement with experiment, the calculated adsorption energy of acridine yellow molecular form is the greatest in case of titania–silica surface where Lewis sites are present, the last one relates to titania surface. For HAY^+, the greatest adsorption energy is a characteristic of titania surface whereas the least one relates to titania–silica surface with Lewis acid sites. Thus, cleavage of methyl and amino groups from acridine yellow molecule occurs with the same probability.

Table 2 Adsorption energy of acridine yellow on the surfaces of TiO_2, SiO_2, and titania–silica films, kJ/mol

Adsorbent surface	Forms of acridine yellow	
	MOLECULAR	Protonated
Silica	−211	−186
Titanium oxide, face(100)	−158	−201
Titania–silica (strong Brønsted site)	−235	−190
Titania–silica (weak Brønsted site)	−223	−194
Titania–silica (Lewis site)	−289	−178

Acridine yellow adsorption and photodegradation on the surface SiO_2, TiO_2 and SiO_2/TiO_2 films observed by UV–Vis and LDI-MS spectra

Adsorption isotherms of AY on the SiO_2, TiO_2 and SiO_2/TiO_2 films demonstrate Langmuir-like behavior. Enhanced adsorption of AY on SiO_2/TiO_2 film coincides with high acidity, surface area and hydrophilicity of synthesized films (Table 1). AY adsorption on the surface of SiO_2 and TiO_2

Table 3 Energy effects of probable destruction routes of gas phase acridine yellow destruction, kJ/mol

Photodestruction route	$\Delta E_{react.}$	
	B3LYP/6–31G(d,p)	B3LYP-D3/6–31G(d,p)
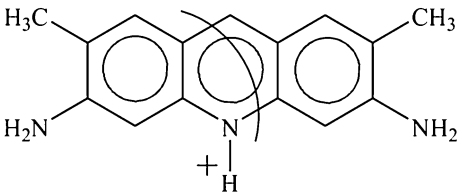 K1	469	426
	598	557

Table 4 Energy effects of acridine yellow photodestruction on various surfaces (kJ/mol)

Surface	Destruction routes	Photodestruction route	
		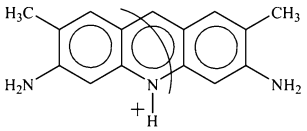 K1	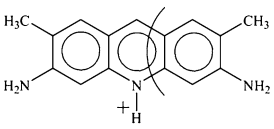 K2
Silica	(*a*)	457	634
	(*b*)	473	614
Titania–silica (Brønsted sites)	(*a*)	464	642
	(*b*)	476	622
Titania–silica (Lewis sites)	(*a*)	502	546
	(*b*)	570	613
Titania (Lewis sites) face(100)	(*a*)	424	493
	(*b*)	405	498

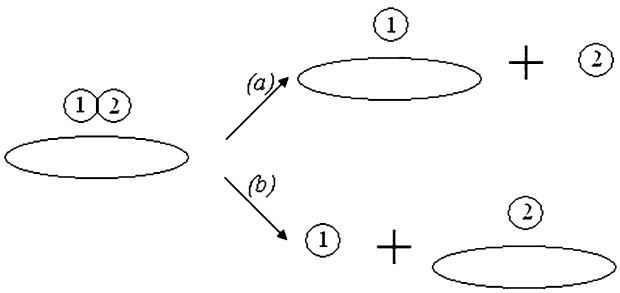

Fig. 10 A scheme of the probable routes of acridine yellow photodestruction in adsorption complexes

films is reversible. Dye molecules can be desorbed easily from TiO_2 and SiO_2 films but cannot be leached from TiO_2/SiO_2 surface by washing in great amount of pure water that can be interpreted in terms of protonation of AY through basic amino groups by acidic OH groups of mixed oxide surface [10] as was observed by us early for AO [48] and 9-aminoacridine on silica surface [49, 50]. These data are in good agreement with our theoretical calculations.

A broad absorption band ($\lambda_{max} = 430$ nm) observed for AY starting aqueous solution (1×10^{-4} M) used for adsorption is a superposition of the spectra of its monomeric and dimeric forms. Dilution of this solution (up to concentration of 1×10^{-6} M) leads to short-wavelength shift of absorption band due to decreasing of dimers concentration [11]. The absorption maximum at 444 nm corresponds to absorption of the monomeric form of AY in solution. However, as was shown for fluorescence excitation spectra of AY adsorbed on SiO_2 surface [51], the dye concentration increase causes a bathochromic shift of the excitation maximum and decreases the emission intensity. It was explained by the formation of various-type associates in the solution and on the oxide surface. The developed porous structure of films is geometrically

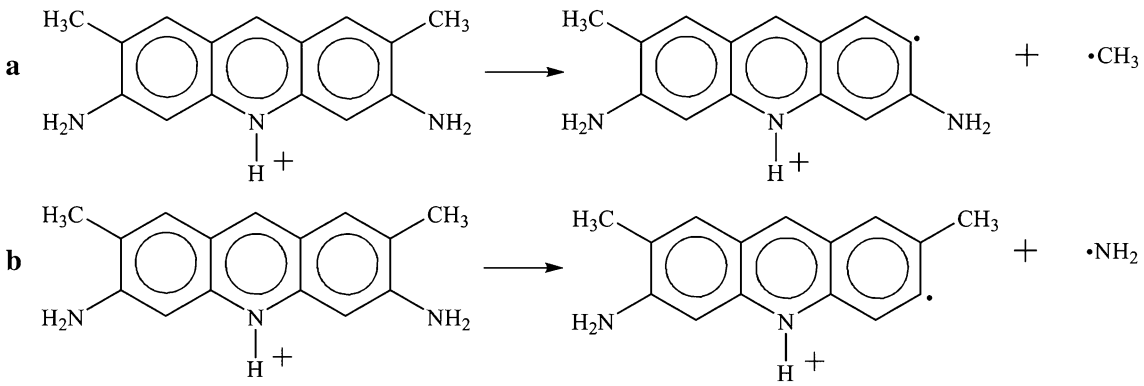

Fig. 11 Elimination reactions of methyl (**a**) and aminogroup (**b**) from acridine yellow molecule

favorable for the adsorption of two and more dye molecules. Associates are formed [48, 49] starting from the covering of ~0.01 % of monolayer what is also confirmed by the presence of peaks with large masses in initial (measured before irradiation) mass spectra (Fig. 12).

The absorption maximum positions of AY dye spectra before irradiation vary with the different synthesized films (Figs. 13, 14, 15a). Monomolecular adsorption of AY with maximum near 442 nm is observed on TiO_2 surface. The short-wave shift of AY absorption bands on the surface of SiO_2 ($\lambda_{max} = 430$ nm) and TiO_2/SiO_2 ($\lambda_{max} = 435$ nm) films with stronger acid sites can be a result of both protonation and dimerization of dye molecules. It is known that protonation of acridine dyes proceed via first proton coordination to nitrogen atom of aromatic ring, causing a bathochromic shift of the absorption spectrum [11]. Further protonation of AY through basic *N*-dimethylamino groups with formation of double ions is accompanied by a shift of the absorption band towards shorter wavelengths. The proton affinity of pyridine nitrogen atom was found theoretically to be 180 kJ/mol greater than that of amine atom.

Irradiation of adsorbed AY in the presence of oxygen leads to a decrease in adsorption intensity and to a long-wave shift of the main absorption band of dye on the SiO_2 and TiO_2 surfaces, whereas on the SiO_2/TiO_2 film a short-wave shift up to 412 nm takes place. Along with a decrease in the main absorption band intensity due to irradiation, an increase in absorption in the 330–340 nm spectral regions (acridine-like absorption) for all the samples is observed. Acridine yellow is capable of forming protonated ions, dimers, and aggregates with corresponding spectral transformations; it is almost impossible to separate these processes relying only on the absorption measurements. Therefore, LDI mass spectra of the samples exposed to UV irradiation for different time intervals (from 0 to 120 min) were obtained and analyzed. It has been found that exposure of three types of films with AY adsorbed to UV light leads to characteristic and reproducible changes in the mass spectra probably associated with different stages of photodegradation of the dye.

Major peaks of the dye cation M^+ with *m/z* 237 and peaks in the mass region close to dimer mass were registered in the LDI mass spectra (Fig. 12, positive ions) of the initial air-dried films with adsorbed AY. The monoisotopic peak of the cation M^+ (*m/z* 237) is accompanied by peaks of $[M+1]^+$ (*m/z* 238) and $[M+2]^+$ (*m/z* 239) with intensities higher than the value expected from the contribution of ^{13}C isotope. The molecular peak M^+ is negligible in LDI spectra of AY adsorbed on TiO_2 films. In the region of large masses, several peaks of varying intensity were observed. A pronounced peak with the mass equal to that of the dimer $2M^+$ (*m/z* 474) was present in LDI spectra of AY adsorbed on TiO_2 and TiO_2/SiO_2 films.

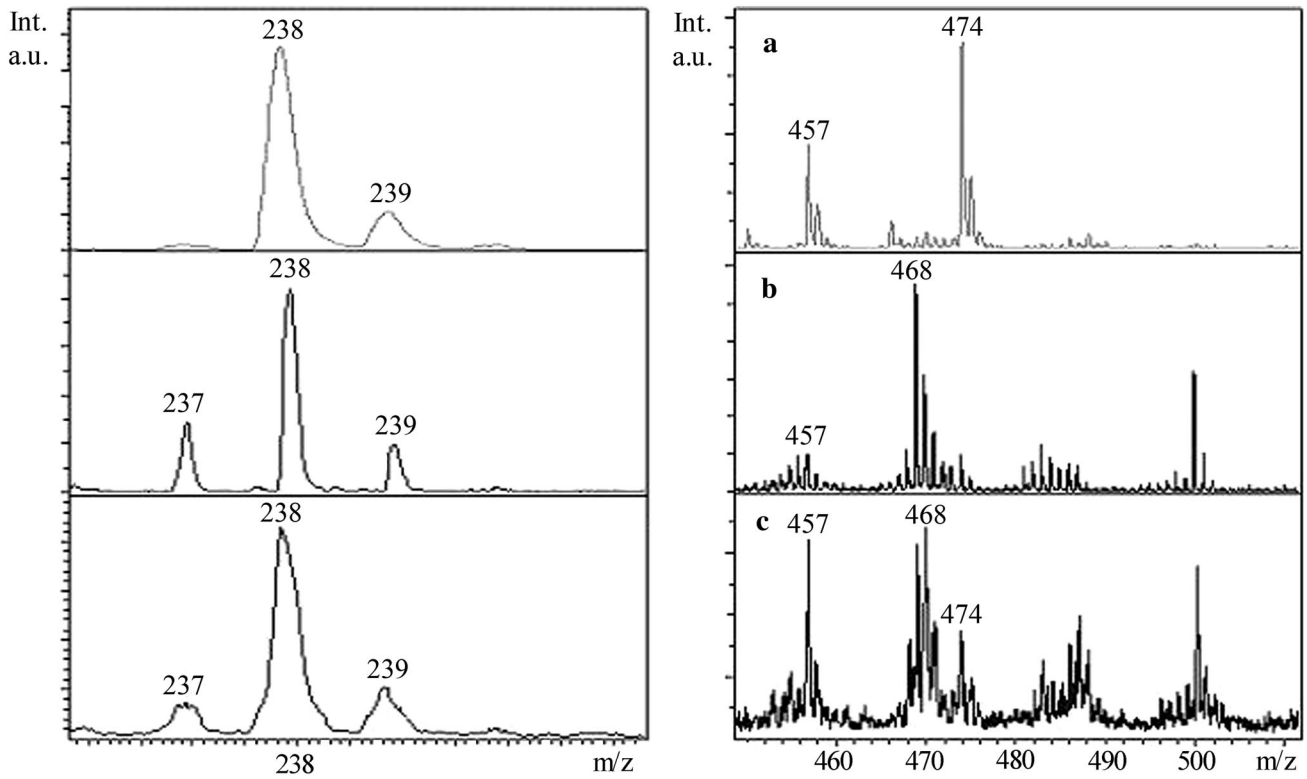

Fig. 12 Initial LDI-MS spectra of AY adsorbed on the A-TiO_2, B-SiO_2 and C-SiO_2/TiO_2 surfaces

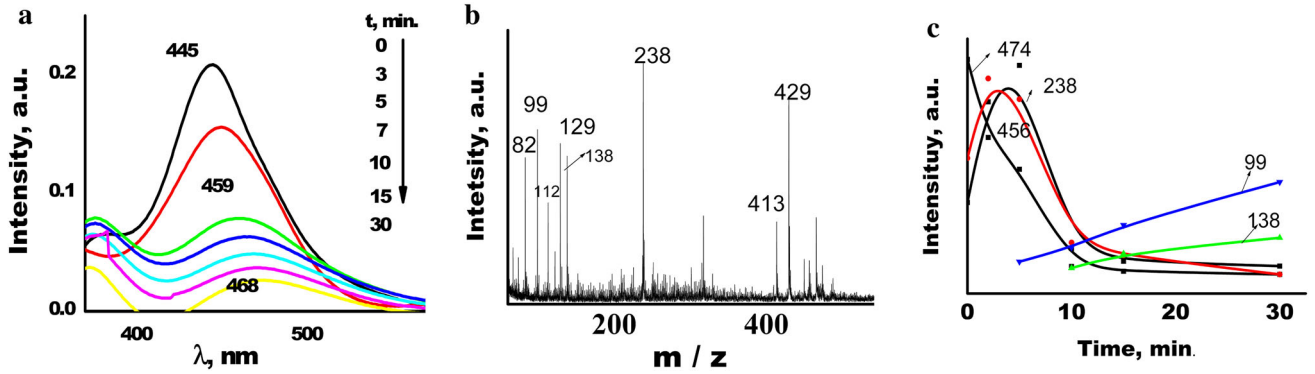

Fig. 13 Evolution of absorption (**a**) and LDI (**b**) spectra after 30 min irradiation of AY on the surface of mesoporous TiO_2 films. Peak intensity of some AY fragments during UV irradiation (**c**)

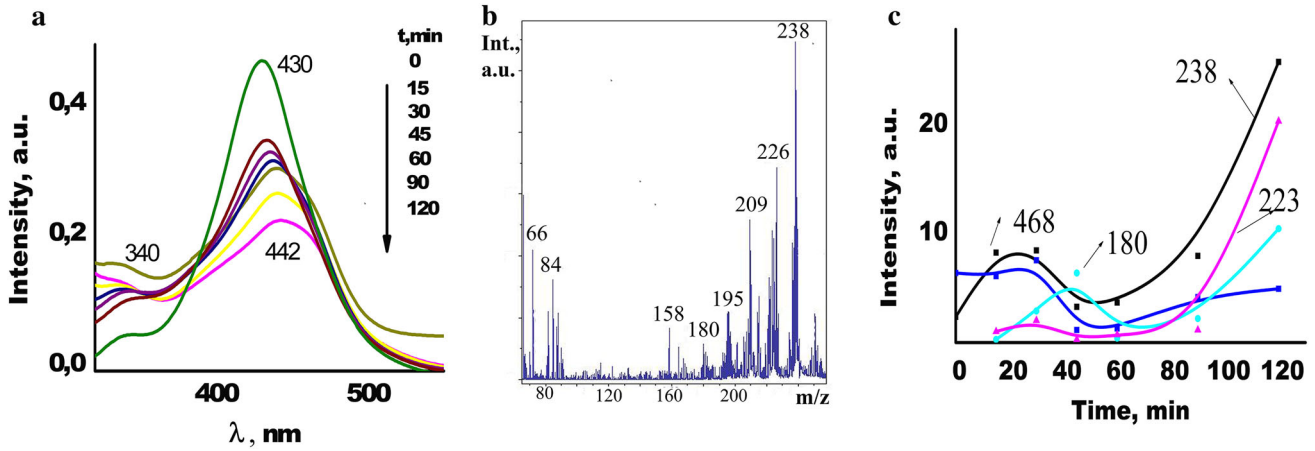

Fig. 14 Evolution of absorption (**a**) and LDI-MS (**b**) spectra after 120 min irradiation of AY on the surface of mesoporous SiO_2 films. Peak intensity of AY fragments during UV irradiation (**c**)

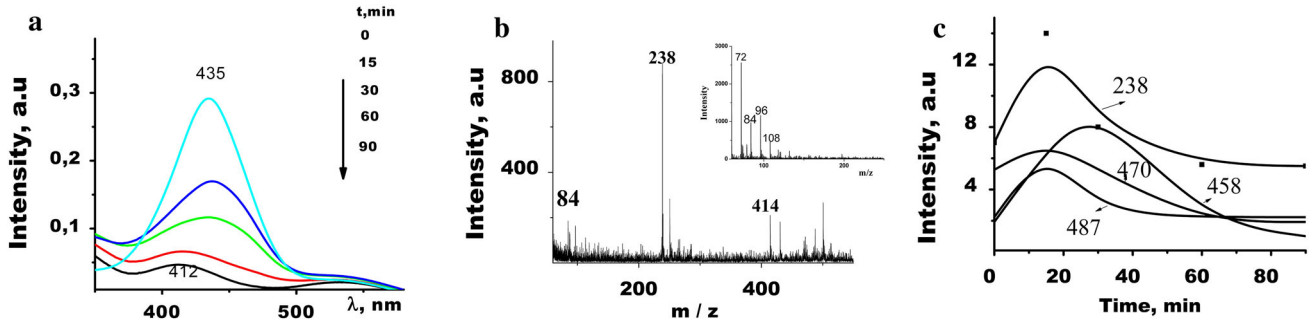

Fig. 15 Evolution of absorption (**a**) and LDI-MS (**b**) spectra after 90 min irradiation of AY on the surface of mesoporous SiO_2/TiO_2 films (*inset* shows negative mode). Peak intensity of AY fragments during UV irradiation (**c**)

The magnitude of the peak of protonated form $[M+1]^+$ (*m/z* 238) increases dramatically in the spectra of all investigated samples under the influence of UV irradiation (5 min for AY adsorbed on TiO_2 and 15—on SiO_2 and TiO_2/SiO_2 films). The optical density at the absorption band maximum decreased by 50 % after irradiation of AY adsorbed on TiO_2 film for 30 min. Since the electron transfer into the TiO_2 conductive band with the cation-radical formation is the first stage of photocatalysed destruction of the dye, it was highly probable that further photodegradation of AY occurred through a radical mechanism [16]. Thus, radicals formed after the loss

of an amino group ($m/z = 223$) were bound to dye molecules to form dimeric aggregates. This was accompanied by a long-wavelength shift of the absorption band maximum to 459 nm (Fig. 13a). Peaks of the corresponding masses ($m/z = 456, 460, 468, 474$) increased in the mass spectrum (Fig. 13c). This process may be explained by protonation of the side amino groups of AY despite the fact that the short-wavelength shift in the absorption spectrum was masked by absorption of the dimers [13, 14]. UV radiation affected mainly highly delocalized electrons of C=C- and C–N- bonds in the dyes leading to photodegradation.

As it has been mentioned above, dye monomers and dimers are present on the film surface. With the onset of irradiation (the first 2–5 min), multiple processes run as follows: (1) breaking of the dimer followed by its protonation which contributes to the sharp increase in the peak of *m/z* 238 (Fig. 13c); (2) increase in the surface hydrophilicity that not only leads to the formation of dimers but also associates with the masses over *m/z* 650–700. In the electronic spectra, this process manifests itself in a shift of the absorption band maximum to longer wavelengths [12] characteristic of the formation of j-aggregates (brickwork) (3) decomposition of AY with the formation of deaminated and demethylated short-lived species (not recorded in the mass spectra) binding to the protonated cation as judged from the increase in the *m/z* 456 peak (Fig. 13c).

This observation agrees well with the results of our theoretical calculations that show similar values of cleavage energy of amino and methyl group; such a cleavage is the first step of AY degradation. Subsequent irradiation leads to a monotonic decrease in the intensity of peaks with large masses in the LDI spectra as well as emergence and increase in peaks with masses less than that of the AY cation (138, 122, 113, 99, 83, 67, etc.), i.e., degradation and mineralization proceed (Fig. 14c). These masses relate to the AY destruction routes predicted theoretically.

While the processes observed on the TiO_2 film are photocatalytic, a slow photolytic decomposition of acridine yellow is observed on the surface of SiO_2 film (Fig. 15).

In this case, multiple stages dominating over other processes can be identified: (1) detachment of amino (peak *m/z* 223) and methyl groups and formation of acridine (peak *m/z* 180) appeared after 15 min of UV exposure (Fig. 15b). It should be mentioned that after 120 min of exposure the mass spectrum still contains peaks corresponding to all stages of cleavage of two amino groups and two methyl groups with the masses of 238, 223, 208, 194, 180; (2) formation of a huge number of dimer associates with the masses of *m/z* 450–500 difficult to identify and group of peaks with masses of *m/z* 700 observed after 45 min of irradiation; (3) decomposition of associates with formation of a molecular cations and degradation products with masses less than *m/z* 180 so indicating destruction of acridine and benzene rings (*m/z* 158, 122, 108, 88, 72, 66, 64) (Fig. 15c).

Most peaks in LDI-MS spectra of AY adsorbed on the mixed oxide surface are much less intensive (under the same laser power) than those on parent oxide surfaces. It is worse noting some peculiarities of photodegradation processes occurred on the TiO_2/SiO_2 film surface. It is essential that during the irradiation no peak with masses more than *m/z* 500 was registered; most decomposition products were observed in the mass spectra of negative ions (Fig. 15, inset). The constants of AY photodegradation rate k_0 evaluated from an inclination of the kinetic curves given in the Table 1 on TiO_2/SiO_2 are almost six times higher than that for SiO_2 film.

Based on theoretical prediction and investigation of absorption spectra and LDI-MS data on AY degradation on the surfaces of mesoporous TiO_2, SiO_2 and TiO_2/SiO_2 films, following scheme (Fig. 16) illustrating these processes can be proposed:

Photodegradation of AY dye adsorbed on the film surface is characterized by different ways of bleaching—a fast process involving photocatalysts on TiO_2 and TiO_2/SiO_2 films containing anatase nanoparticles (half-time of degradation 4 and 15 min, respectively), or a slow process (more than 90 min) of chemical oxidation of protonated via aminogroup acridine yellow on silica surface in air.

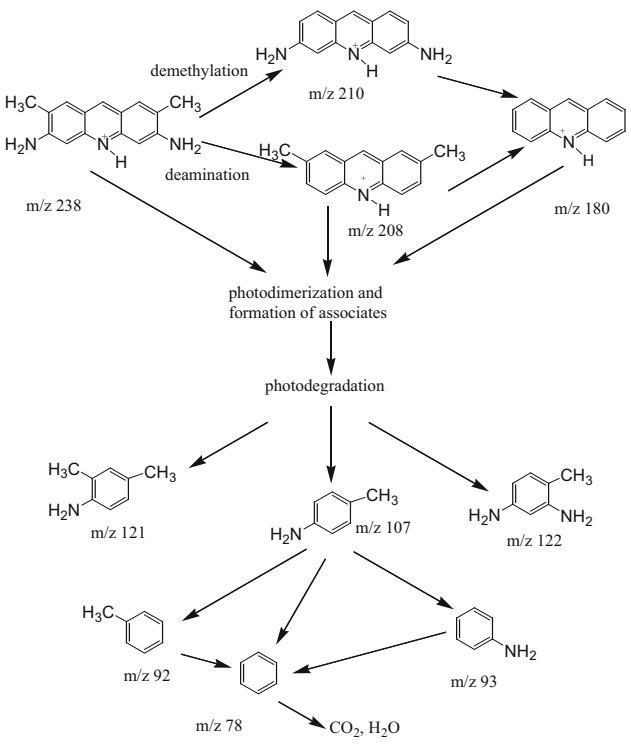

Fig. 16 Scheme of AY photodegradation

Conclusions

Solid transparent mesoporous SiO_2, TiO_2/SiO_2 and TiO_2 films on glass substrates have been synthesized using templated sol–gel method. Acridine yellow is capable of forming protonated ions, dimers, and aggregates with corresponding spectral transformations. Electronic spectroscopy and LDI mass spectrometry investigations have proved that the effectiveness of acridine yellow photodegradation on the surface of mesoporous films under UV irradiation increases in a row $SiO_2 < TiO_2/SiO_2 < TiO_2$. The combination of theoretical modeling, electronic spectroscopy and laser desorption/ionisation mass spectrometry methods facilitates to get a reliable data on the mechanisms and kinetics of dye molecule destruction taking place under UV irradiation on the surface of photocatalytically active mesoporous films. The mechanisms and kinetics of the AY photodegradation are determined by the surface chemistry of the film and the presence of the semiconductor.

References

1. Ullmann's encyclopedia of industrial chemistry. 6th edn. Wiley, New York (2001)
2. Liua, S.P., Sab, C., Hua, X., Konga, L.: Fluorescence quenching method for the determination of sodium carboxymethyl cellulose with acridine yellow or acridine orange. Spectrochimica Acta Part A Mol Biomol Spectrosc **64**, 817–822 (2006)
3. Charmantray, F., Duflos, A., Lhomme, J., et al.: Synthesis and study of 4-hydroxymethyl-3-(alkylamino) acridines as models of a new class of DNA-intercalating-alkylating agents. J. Chem. Soc. Perkin Trans. **1**, 2962–2968 (2001)
4. Zakharenko, V.S., Parmon, V.N.: Efficiency of sensitization of titanium dioxide by adsorbed acridine yellow in photocatalytic hydrogen evolution. React. Kinet. Catal. Lett. **4**, 389–394 (1987)
5. Amata, A.M., Arquesa, A., Galindob, F., Mirandac, M.A., Santos-Juanesa, L., Verchera, R.F., Vicentea, R.: Acridine yellow as solar photocatalyst for enhancing biodegradability and eliminating ferulic acid as model pollutant. Appl Catal B Environ. **73**, 220–226 (1997)
6. Perera, V.P.S., Pitigala, P.K.D.D.P., Jayaweera, P.V.V., Bandaranayake, K.M.P., Tennakone, K.: Dye-sensitized solid-state photovoltaic cells based on dye-multilayer semiconductor nanostructures. J. Phys. Chem. B **107**, 13758–13761 (2010)
7. Bach, U., Lupo, D., Comte, P., Moser, J.E., Weissörtel, F., Salbeck, J., Spreitzer, H., Grätzel, M.: Solid-state dye-sensitized mesoporous TiO_2 solar cells with high photon-to-electron conversion efficiencies. Nature **395**, 583–585 (1998)
8. Kumar, D.A., Shyla, J.M., Xavier, F.P.: Synthesis and characterization of TiO_2/SiO_2 nanocomposites for solar cell applications. Appl. Nanosci. **2**, 1–8 (2012)
9. Worrall, D.R.; Williams, S., Eremenko, A., Smirnova, N., Yakimenko, O., Staruch, G.: Coll. and Surfaces A: Physicochem. Eng. Aspects. 230, 45–55 (2004)
10. Imamura, S., Ishida, S., Tarumoto, H., Saito, Y., Ito, T.: Effect of the composition of titania-silica on its physical and photocatalytic properties. J. Chem. Soc. Faraday Trans. **89**, 757–762 (1993)
11. Vlasova, N.N., Golovkova, L.P., Stukalina, N.G.: Adsorption complexes of acridine diaminoderivatives on the silica surface. Kolloidny Zhournal. **74**, 25–34 (2012)
12. Gallopini, E., Thyagarajan, S.: Organic dyes aggregation on TiO_2 surface. Spectrum. **18**, 25–27 (2005)
13. Rauf, M.A., Ashraf, S.S.: Fundamental principles and application of heterogeneous photocatalytic degradation of dyes in solution. Chem. Eng. J. **151**, 10–18 (2009)
14. Negrón-Encarnación, I., Arce, R.: Light-induced transformations of aza-aromatic pollutants adsorbed on models of atmospheric particulate matter: acridine and 9 (10-H) acridone. Atmos. Environ. **41**, 6771–6783 (2007)
15. Fesenko, T.V., Kosevich, M.V., Surovtseva, N.I., Pokrovsky, V.A., Eremenko, A.M., Smirnova, N.P.: Mass-spectrometry with laser desorption/ionization of methylene blue dye from the surface of mesoporous thin TiO_2, TiO_2/SiO_2 and SiO_2 films. Mass spectrom. **4**, 289–296 (2007)
16. Surovtseva, N.I., Eremenko, A.M., Smirnova, N.P., Pokrovsky, V.A., Fesenko, T.V., Starukh, G.N.: The effect of nanosized titania-silica film composition on the photostability of adsorbed methylene blue dye. Theor. Exp. Chem. **43**, 220–225 (2007)
17. Surovtseva, N., Smirnova, N., Fesenko, T., Gnatyuk, Yu., Eremenko, A., Pokrovsky, V.: Spectroscopic and mass-spectrometric study of acridine orange photodegradation on the surface of mesoporous TiO_2, TiO_2/SiO_2 and SiO_2. J. Adv. Oxid. Technol. **11**, 551–560 (2008)
18. Gnatyuk, Yu., Smirnova, N., Eremenko, A., Ilyin, V.: Design and photocatalytic activity of mesoporous TiO_2/ZrO_2 thin films. Ads. Sci. Technol. **23**, 497–508 (2005)
19. Krylova, G.V., Gnatyuk, YuI, Smirnova, N.P., Eremenko, A.M., Gunko, V.M.: Ag nanoparticles deposited onto silica, titania and zirconia mesoporous films synthesized by sol-gel template method. J. Sol–Gel. Sci. Technol. **50**, 216–228 (2009)
20. Pavlova-Verevkina, O.B., Politova, E.D., Nazarov, V.V.: Preparation and structure of stable dispersions of uniform TiO_2 nanoparticles. Colloid J. **61**, 359–362 (1999)
21. Gregg, S.J., Sing, K.S.W.: Adsorption, Surface Area and Porosity. Academic Press, London (1982)
22. Kruk, M., Jaroniec, M., Sayari, A.: Application of large pore MCM-41 molecular sieves to improve pore size analysis using nitrogen adsorption measurements. Langmuir **13**, 6267–6273 (1997)
23. Wang, R., Hashimoto, K., Fujishima, A., Chikuni, M., Kojima, E., Kitamura, A., Watanabe, T.: Light-induced amphiphilic surfaces. Nature **388**, 431–438 (1997)
24. Sakai, N., Fujishima, A., Watanabe, T., Hashimoto, K.: Quantitative evaluation of the photoinduced hydrophilic conversion properties of TiO_2 thin film surfaces by the reciprocal of contact angle. J. Chem. Phys. **107**, 1028–1036 (2003)
25. Watanabe, T., Kitamura, A., Kojima, E., Nakayama, C., Hashimoto, K., Fujishima, A.: Photocatalytic purification and treatment of water and air. In: Ollis D.F., Al-Ekabi H. (eds.) Elsevier, Amsterdam (1993)
26. Mikushina, YuV, Shishmakov, A.V., Matskevich, V.V., Zhuravlev, N.A., Koryakova, O.V., Kharchuk, V.G., Petrov, L.A.: TiO_2–SiO_2 binary xerogels: synthesis and characterization. Russ. J. Inorg. Chem. **53**, 1557–1560 (2008)

27. Lee, J.W., Kong, S., Kim, W.S., Kim, J.: Preparation and characterization of SiO_2/TiO_2 core-shell particles with controlled shell thickness. Mater. Chem. Phys. **106**, 39–44 (2007)
28. Xiea, C., Xua, Z., Yanga, Q., Xuea, B., Dua, Y., Zhang, J.: Enhanced photocatalytic activity of titania–silica mixed oxide prepared via basic hydrolyzation. Mater. Sci. Eng. B **112**, 34–41 (2004)
29. Jung, W.Y., Baek, S.H., Yang, J.S., Lim, K.-T., Lee, M.S., Lee, G.-D., Park, S.S., Hong, S.-S.: Synthesis of Ti-containing SBA-15 materials and studies on their photocatalytic decomposition of orange II. Catal. Today **131**, 437–443 (2008)
30. Salehirad, F., Aghabozorg, H.R., Manoochehri, M., Aghabozorg, H.: Catalysis communications. Ref. Data **5**, 359–365 (2004)
31. Lin, K., Sun, Z., Lin, S., Jiang, D., Xiao, F.-S.: Ordered mesoporous titanosilicates with better catalytically active titanium sites assembled from preformed titanosilicate precursors with zeolite building units in alkaline media. Microporous Mesoporous Mater. **72**(1–3), 193–201 (2004)
32. Galán-Fereres, M., Alemany, L.J., Mariscal, R., Bañares, M.A., Anderson, J.A., Fierro, J.L.G.: Surface acidity and properties of titania-silica catalysts. Chem. Mater. **7**, 1342–1348 (1995)
33. Andrulevičius, M., Tamulevičius, S., Gnatyuk, Yu., Vityuk, N., Smirnova, N., Eremenko, A.: XPS investigation of $TiO_2/ZrO_2/SiO_2$ films modified with Ag/Au nanoparticles. Mater Sci. (Medžiagotyra). **14**, 8–14 (2008)
34. San, N., Hatipoğlu, A., Koçtürk, G., Çınar, Z.: Photocatalytic degradation of 4-nitrophenol in aqueous TiO2 suspensions: theoretical prediction of the intermediates. J. Photochem. Photobiol A Chem. **146**, 189–197 (2002)
35. Katajisto, J., Pakkanen, T.T., Tapani Pakkanen, A., Hirva, P.: Ab initio study on thermal degradation reactions of polycarbonate. J. Mol. Structure (Theochem) **634**, 305–310 (2003)
36. Demianenko, E., Ilchenko, M., Grebenyuk, A., Lobanov, V., Tsendra, O.: A theoretical study on ascorbic acid dissociation in water clusters. J. Mol. Model. **20**, 2128–2132 (2014). doi:10.1007/s00894-014-2128-5
37. Becke, A.D.: Density functional thermochemistry. III. The role of exact exchange. J. Chem. Phys. **98**, 5648–5661 (1993). doi:10.1063/1.464913
38. Lee, C., Yang, W., Parr, R.G.: Development of the Colle-Salvetti correlation-energy formula into a functional of the electron density. Phys. Rev. B. **37**, 785–789 (1988)
39. Grimme, S., Ehrlich, S., Goerigk, L.: Effect of the damping function in dispersion corrected density functional theory. J. Comput. Chem. **32**, 1456–1465 (2011). doi:10.1002/jcc.21759
40. Schmidt, W., Baldrige, K.K., Boatz, J.A., Elbert, S.T., Gordon, M.S., Jensen, J.H., Koseki, S., Matsunaga, N., Nguyen, K.A., Su, S., Windus, T.L., Dupuis, M., Montgomery, J.A.: General atomic and molecular electronic structure system. J. Comput. Chem. **14**, 1347–1363 (1993). doi:10.1002/jcc.540141112
41. Sinclair, P.E., Richard, C., Catlow, A.: On the formation of titanyl (Ti=O) groups in mesoporous and microporous titanosilicate catalysts: a computational study. Chem. Commun. (19), 1881–1882 (1997). doi:10.1039/A704567K
42. Libau, F.: Structural Chemistry of Silicates. Springer, New York (1985)
43. Fahmi, A., Causá, C.M.B.S.M.: Theoretical analysis of the structures of titanium dioxide crystals. Phys. Rev. B. **47**, 11717–11724 (1993)
44. Klessinger, M.: Theoretical models for the selectivity of organic singlet and triplet photoreactions. Pure Appl. Chem. **69**(4), 773–778 (1997)
45. Fesenko, T.V., Pokrovskiy, V.A., Surovtseva, N.I., Eremenko, A.M., Smirnova, N.P., Boryak, O.A., Selkovsky, V.S., Kosevich, M.V.: Laser desorption/ionization mass-spectrometry of acridine dyes adsorbed on the surface of TiO_2 and SiO_2 films. Surface. **1**(16), 125–135 (2009)
46. Pankratov, A.N., Uchaeva, I.M.: A semiempirical quantum chemical testing of thermodynamic and molecular properties of arsenic compounds. J. Mol. Struct. THEOCHEM. **498**, 247–254 (2000)
47. Murashov, V.: Ab initio cluster calculations of silica surface sites. J. Mol. Struct. **650**, 141–157 (2003)
48. Surovtseva, N.I., Smirnova, N.P., Fesenko, T.V., Gnatyuk, YuI, Eremenko, A.M., Pokrovskiy, V.A.: Spectroscopic and mass-spectrometric study of organic dyes photodegradation on the surface of mesoporous TiO_2, SiO_2/TiO_2 and SiO_2 films. J Adv Oxid Technol. **11**, 551–560 (2008)
49. Eremenko, A.M., Smirnova, N.P., Ogenko, V.M., Chuiko, A.A.: Luminescence of organic dyes in silica matrices. Res. Chem. Intermed. **19**, 855–864 (1993)
50. Smirnova, N., Eremenko, A., Bykovskaya, L., Kulikov, S., Chuiko, A.: Fluorescence spectra of adsorbed heteroaromatic molecules at selective laser excitation. J. Mol. Struct. **266**, 417–422 (1992)
51. Runov, V.K.: State of Rhodamine dyes and acridine yellow on the silica surface. Physical chemistry of surface phenomena. Zh. Fiz. Khim. **72**, 933–937 (1998)